



Constraining the γ -Ray Emission Region for Fermi-detected FSRQs by the Seed Photon Approach

Danyi Huang¹, Ziyang Li¹, Jiru Liao¹, Xiulin Huang¹, Chengfeng Li¹, Yanjun Qian¹, Zhiyuan Pei^{1,2,3,4}, and Junhui Fan^{1,2,3,4}

¹School of Physics and Materials Science, Guangzhou University, Guangzhou 510006, People's Republic of China; peizy@gzhu.edu.cn, fjh@gzhu.edu.cn

²Center for Astrophysics, Guangzhou University, Guangzhou 510006, People's Republic of China

³Astronomy Science and Technology Research Laboratory of Department of Education of Guangdong Province, Guangzhou 510006, People's Republic of China

⁴Key Laboratory for Astronomical Observation and Technology of Guangzhou, Guangzhou 510006, People's Republic of China

Received 2022 March 28; accepted 2022 July 13; published 2022 August 18

Abstract

The location of γ -ray-emitting region in blazars has been an open issue for several decades and is still being debated. We use the Paliya et al. sample of 619 γ -ray-loud flat-spectrum radio quasars with available spectral energy distributions and employ a seed photon factor approach to locate the γ -ray production region. This method efficiently sets up a relation between the peak frequencies and luminosities for the synchrotron emission and inverse Compton scattering, together with a combination of the energy density and characteristic energy for the external seed photon field, namely, $\sqrt{U_0}/\epsilon_0$, an indicative factor of seed photons in units of Gauss. By comparing it with canonical values of the broad-line region (BLR) and molecular dusty torus (DT), we principally ascertain that the GeV emission originated far beyond the BLR and close to the DT—farther out at parsec scales from the central black hole, which supports a far-site scenario for γ -ray blazars. We probe the idea that inverse Compton scattering of infrared seed photons is happening in the Thomson regime. This approach and our findings are based on the validity of the external Compton model, which is applicable in understanding the GeV emission mechanism in FSRQs. However, the completeness of this framework has been challenged by reports of neutrino emission from blazars. Thus, we also shed new light on the neutrino production region by using our derived results because blazars are promising neutrino emitters.

Unified Astronomy Thesaurus concepts: [Active galaxies \(17\)](#); [Flat-spectrum radio quasars \(2163\)](#); [Gamma-ray sources \(633\)](#)

Online material: machine-readable table

1. Introduction

As the most distinctive subclass of active galactic nuclei (AGNs), blazars are characterized by high-amplitude rapid variability, apparent superluminal motion in their parsec-scale jet, core-dominated nonthermal continuum, and strong emission over the entire electromagnetic spectrum because their relativistic jets are oriented very close to the observer's line of sight (Wills et al. 1992; Urry & Padovani 1995; Romero et al. 2002; Fan et al. 2005, 2016, 2021; Abdo et al. 2010a, 2010b; Ghisellini et al. 2010; Marscher et al. 2011; Acero et al. 2015; Pei et al. 2016, 2020a, 2020b; Xiao et al. 2019; Ajello et al. 2020; Burd et al. 2021), and all of these properties are due to the relativistic beaming effect (Madau et al. 1987; Ghisellini 1993; Dondi & Ghisellini 1995; Fan et al. 2009, 2013; Savolainen et al. 2010; Pei et al. 2019; Yang et al. 2022).

Historically, featuring the appearance of the broad emission lines in their optical spectra, blazars are divided into two categories: flat-spectrum radio quasars (FSRQs), which exhibit strong and broad emission lines with an equivalent width of $EW > 5 \text{ \AA}$ in the rest-frame, and BL Lacertae objects (BL Lacs), which have

quasi-featureless spectra ($EW < 5 \text{ \AA}$) (Urry & Padovani 1995; Scarpa & Falomo 1997). Alternatively, the demarcation between two subclasses can be drawn based on the luminosity of the broad-line region (BLR) of FSRQs measured in Eddington units: $L_{\text{BLR}}/L_{\text{Edd}} \gtrsim 5 \times 10^{-4}$, i.e., $L_{\text{Disk}}/L_{\text{Edd}} \gtrsim 5 \times 10^{-3}$, when $L_{\text{BLR}} \simeq 0.1L_{\text{Disk}}$ is taken into account, while BL Lacs have luminosity lower than this criterion (Ghisellini et al. 2011; Pei et al. 2022). Here L_{BLR} , L_{Disk} , and L_{Edd} denote the BLR luminosity, accretion luminosity, and Eddington luminosity, respectively. This more physical classification indicates that FSRQs may have stronger accretion disk emission.

The spectral energy distributions (SEDs) of blazars are usually dominated by two spectral peaks: the first at low to medium energies (radio to X-ray, $\nu^p \sim 10^{13} \text{ Hz}$), and the second at high energies (from X-ray to γ -ray, $\nu^p \sim 10^{22} \text{ Hz}$) (see, e.g., Ghisellini et al. 1998; Fan et al. 2016, and references therein). Based on the leptonic blazar model, the first peak is produced by synchrotron emission from ultrarelativistic electrons embedded in a magnetic field within the plasma jet, and the second peak is believed to emanate from the inverse

Compton (IC) scattering of low-energy photons by the same electron population that generates the synchrotron emission (Fossati et al. 1998; Ghisellini et al. 1998; Böttcher 1999; Chen 2018). The GeV emission is generally believed to be generated by IC emission.

Blazars dominate the extragalactic γ -ray sky (Abdo et al. 2010c, 2010d; Abdollahi et al. 2020; Fermi-LAT collaboration et al. 2022). However, the question of the dominant production mechanism and exact location of the γ -ray emission observed in blazars has remained unresolved for several decades. The lack of high-resolution instruments and the complicated nature of blazars have resulted in plenty of proposals about the γ -ray emission region.

Regarding FSRQs, it is generally accepted that γ -ray photons are probably attributable to the IC scattering of external ambient photon fields (EC). Two scenarios have been discussed, namely near-site, i.e., inside the BLR, in which the dissipated energy is located at a distance of $\lesssim 0.1$ –1 pc from a central supermassive black hole (SMBH) (see e.g., Sikora et al. 1994; Poutanen & Stern 2010), and/or far-site, i.e., outside the BLR or beyond the molecular dusty torus (DT), in which the electron energy is dissipated several parsecs away from the SMBH (e.g., Wagner et al. 1995; Błażejowski et al. 2000; Jorstad et al. 2001; Arbeiter et al. 2002; Marscher et al. 2010; Meyer et al. 2019).

The critical difference between the BLR and DT is the energy of the seed photons. If the GeV emission originates within the BLR, the IC scattering of ultraviolet (UV) seed photons that produces the γ -rays occurs at the onset of the Klein–Nishima regime. On the other side, if the γ -ray emission is produced farther out in the DT, then the IC scattering of infrared (IR) seed photons comes from the Thomson regime.

The Large Area Telescope on board the Fermi Gamma-ray Space Telescope (Fermi-LAT) provided, for the first time, γ -ray light curves and has been detecting flares with variability timescales of $\sim 10^4$ s in some FSRQs since its launch in 2008, offering evidence of γ -ray emission produced in the near-site scenario (Abdo et al. 2009a, 2010c, 2010e; Atwood et al. 2009; Ackermann et al. 2010; Foschini 2011; Nalewajko et al. 2014). By analyzing the light curves of two FSRQs, 3C 454.3 and PKS 1510–089, Tavecchio et al. (2010) discussed the implications of significant variability on short timescales that have challenged the scenario that γ -rays are produced in regions of the jet at large distances (tens of parsecs) from the black hole.

Studies of blazars in the radio band or very long baseline interferometry (VLBI) monitoring programs suggest that the γ -ray and VLBI jet emission are cospatial, supporting the idea of a far-site scenario (e.g., Larionov et al. 2008; Sikora et al. 2008; Jorstad et al. 2010; Marscher et al. 2010; Agudo et al. 2011). Zheng et al. (2017) studied 36 FSRQs by modeling their SEDs and came to the conclusion that the γ -ray-emitting regions of FSRQs are located closer to the dusty DT ranges than the BLR.

Applying a similar method to SED modeling, Cao & Wang (2013) inferred that the location of the GeV emission region is outside the DT for three-quarters of selected FSRQs in their sample. Lindfors et al. (2005) analyzed 3C 279, one of the best-observed blazars, proposing that a significant external seed photon field is provided by the DT, which extends farther than the BLR. Quite recently, Kramarenko et al. (2022) derived the deprojected distance between the central engine and the region of the GeV emission for 46 γ -ray-bright blazars by exploring the correlation between the 15 GHz VLBA flux densities and the γ -ray photon flux. They ascertained that the seed photons responsible for the γ -ray emission are likely to originate well beyond the BLR, located at a distance of a few parsecs from the central engine.

In this paper, we aim to determine the location of GeV emission for the γ -ray FSRQs. We follow an effective method first proposed by Georganopoulos et al. (2012), namely the seed photon factor (SF), and constrain the location of energy dissipation for an enlarged sample of FSRQs. This paper is organized as follows. The approach we apply is going to be well presented in Section 2. In Section 3 we describe our sample and the derived results. We conduct a statistical analysis and discuss in Section 4. Finally, we summarize our main findings in Section 5. Throughout this paper, we adopt the Λ CDM model with $\Omega_\Lambda \simeq 0.73$, $\Omega_M \simeq 0.27$, and $H_0 \simeq 68$ km s^{-1} Mpc $^{-1}$ (Planck Collaboration et al. 2014). The logarithms we employ in all equations below are in the base of 10.

2. Method

2.1. Model Description

The peak energy of synchrotron emission and the EC scattering in the observer frame can be expressed as

$$\epsilon_{\text{syn}} = \frac{B}{B_{\text{cr}}} \gamma_b^2 \delta / (1 + z), \quad (1)$$

$$\epsilon_{\text{EC}} = \frac{4}{3} \epsilon_0 \gamma_b^2 \delta^2 / (1 + z), \quad (2)$$

respectively (Coppi & Blandford 1990; Tavecchio et al. 1998; Ghisellini & Tavecchio 2008), where δ is the Doppler factor of the jet, defined by $\delta = [\Gamma(1 - \beta \cos \theta)]^{-1}$, $\beta = v/c$ denotes the speed of electrons in units of the speed of light c , $\Gamma = (1 - \beta^2)^{-1/2}$ is the bulk Lorentz factor, and θ signifies the viewing angle. γ_b is the Lorentz factor of the electrons responsible for the synchrotron and EC components, ϵ_0 is the characteristic energy of the external seed photons, B is the magnetic field permeating the emission region within the jet, and $B_{\text{cr}} = m_e c^3 / e \hbar = 4.4 \times 10^{13}$ G is the critical magnetic field. ϵ_{syn} and ϵ_{EC} are both in units of electron rest-mass energy.

Taking the ratio of the two peak energies, we obtain

$$\frac{B}{\delta} = \frac{4\epsilon_0 \epsilon_{\text{syn}} B_{\text{cr}}}{3\epsilon_{\text{EC}}}. \quad (3)$$

The observed synchrotron peak luminosity and the observed peak IC luminosity are given by Blumenthal & Gould (1970) and Rybicki et al. (1981):

$$L_{\text{syn}} = \frac{4}{3} \sigma_T c \beta \gamma_b^2 n(\gamma_b) U_B \delta^4, \quad (4)$$

$$L_{\text{IC}} = \frac{16}{9} \sigma_T c \beta \gamma_b^2 n(\gamma_b) U_0 \delta^6, \quad (5)$$

here σ_T is the Thomson cross section, $n(\gamma_b)$ is the electron energy distribution at γ_b , U_0 is the external photon field energy density in the galaxy frame, defined by $U_0 = \frac{3}{4} U'_0 / \Gamma^2$, where Γ is the bulk Lorentz factor, U'_0 is the external photon field energy density in the jet comoving frame, and $U_B = B^2 / 8\pi$ is the magnetic field energy density.

The ratio of Equation (4) to Equation (5) is a well-known parameter—the Compton dominance (CD),

$$\text{CD} = \frac{L_{\text{IC}}}{L_{\text{syn}}} = \frac{32\pi\delta^2 U_0}{3B^2}. \quad (6)$$

Substituting Equation (3) into Equation (6), one can read

$$\frac{U_0}{\epsilon_0^2} = \frac{\text{CD}}{6\pi} \frac{\epsilon_{\text{EC}}^2}{\epsilon_{\text{syn}}^2} B_{\text{cr}}^2 \quad (7)$$

$$\Rightarrow \frac{\sqrt{U_0}}{\epsilon_0} = 10120 \times \frac{\sqrt{\text{CD}} \nu_{\text{syn},13}^{\text{p}}}{\nu_{\text{EC},22}^{\text{p}}}, \quad (8)$$

where $\nu_{\text{syn},13}^{\text{p}}$ and $\nu_{\text{EC},22}^{\text{p}}$ signify the peak frequency of synchrotron/IC component in units of 10^{13} Hz and 10^{22} Hz, respectively.

Therefore, the seed photon factor (SF) can be given as $\log \sqrt{U_0} / \epsilon_0$, i.e.,

$$\text{SF} = \log \frac{\sqrt{U_0}}{\epsilon_0} = \log \left(10120 \times \frac{\sqrt{\text{CD}} \nu_{\text{syn},13}^{\text{p}}}{\nu_{\text{EC},22}^{\text{p}}} \right) \text{G}. \quad (9)$$

Here we remark that U_0 and ϵ_0 denote the energy density and characteristic photon energy of the external seed photon population, respectively, the former parameter being in units of erg cm^{-3} and the latter one in units of the electron rest mass. Because $1 \text{ erg} = 1 \text{ cm}^2 \text{ g s}^{-2}$ in cgs units, $\text{SF} = \log \sqrt{U_0} / \epsilon_0$ will thus be in units of $\text{cm}^{-1/2} \text{ g}^{1/2} \text{ s}^{-1}$, i.e., Gauss. This also can be easily seen from Equation (7) that $\sqrt{U_0} / \epsilon_0$ has units consistent with B_{cr} , which is in Gauss. Furthermore, this seed photon approach is only applicable to the EC emission model because our derived estimation of the SF is fully based on Equation (2). Therefore, we only make use of this method when discussing FSRQ-type blazars.

This diagnostic is robust. The value of the SF for a specific source can be determined as long as four physical parameters from the broadband SEDs are available. These are the peak frequency and peak luminosity of the synchrotron emission and IC scattering (the latter can be transformed to CD). Note that these quantities are observable and can be obtained directly from the quasi-simultaneous multiwavelength SED modeling or other reference. Quasi-simultaneous SEDs guarantee that the biases can be minimized due to averaging and reduce the chance of interband integration mismatches. In other words, quasi-simultaneous SEDs are unlikely to have X-ray data during a high state while other data are taken during a low state.

The seed factor is believed to owe to the EC scattering on a specific photon population, hinging on the energy density and characteristic photon energy of the upscattered seed photon population. They are known very well for both the BLR and DT. Thus, after the SF value for a source is determined, we can compare it with the canonical SF values of the BLR and DT, and thereby constrain the location of the γ -ray emission for this source.

2.2. Characteristic Values of the Seed Factor for the Broad-line Region and Molecular Torus

In this paper, for canonical SF values of the BLR, we follow the calculation in Georganopoulos et al. (2012). Reverberation mapping of the BLR points to a typical size of $R_{\text{BLR}} \approx (1 \sim 3) \times 10^{17} L_{d,45}^{1/2} \text{ cm}$ (Kaspi et al. 2007; Bentz et al. 2009) for AGNs, where $L_{d,45}$ denotes the accretion disk luminosity in units of $10^{45} \text{ erg s}^{-1}$. The energy density of the BLR can be estimated as $U_{0,\text{BLR}} = \xi L_d / (4\pi R_{\text{BLR}}^2) \simeq (0.3\text{--}2.6) \times 10^{-2} \text{ erg cm}^{-3}$, here ξ is the BLR covering factor, and we take $\xi = 0.1$ in our calculation (Ghisellini & Tavecchio 2009). The value of $U_{0,\text{BLR}}$ can be considered to be the same among different sources. Because the BLR SED in the galaxy frame can be approximated by a blackbody with a peak frequency of $\nu_{\text{BLR}} = 1.5\nu_{L_x}$ (Tavecchio & Ghisellini 2008), consequently the characteristic photon energy of the BLR is $\epsilon_{0,\text{BLR}} = 3 \times 10^{-5}$ in units of the electron rest mass. Using these, one can obtain the canonical SF values of the BLR to be $\text{SF}_{\text{BLR}} = \log \sqrt{U_{0,\text{BLR}}} / \epsilon_{0,\text{BLR}} \simeq 3.26\text{--}3.74 \text{ G}$ (Georganopoulos et al. 2012). A similar result can be found in Harvey et al. (2020).

In the molecular torus, reverberation mapping and near-infrared interferometric studies have been normally effective for radio-quiet sources, e.g., Seyfert galaxies and low-luminosity blazars, due to their smaller DT region (e.g., Suganuma et al. 2006; Kishimoto et al. 2011; Pozo Nuñez et al. 2014). However, we assume that the relation that the radius of the DT scales proportionally to $L_{d,45}^{1/2}$ holds for our sample of FSRQs, i.e., $R_{\text{DT}} \approx 2.5 \times 10^{18} L_{d,45}^{1/2} \text{ cm}$ (see e.g., Ghisellini & Tavecchio 2009; Yan et al. 2018; Pei et al. 2022). The energy density of DT therefore can be estimated

by $U_{0,DT} \simeq 3.91 \times 10^{-3} - 1.42 \times 10^{-2} \text{ erg cm}^{-3}$. The molecular torus spectrum can be approximated using a blackbody spectrum with a temperature of $T = 1200 \text{ K}$ (Malmrose et al. 2011; Georganopoulos et al. 2012; Harvey et al. 2020), which leads to the characteristic photon energy for the DT of $\epsilon_{0,DT} = 5.7 \times 10^{-7}$. Hence, we obtain the canonical SF values of DT to be $SF_{DT} = \log \sqrt{U_{0,DT}} / \epsilon_{0,DT} \simeq 5.04 - 5.32 \text{ G}$.

3. Sample and Results

3.1. Sample

To study the black hole mass (M_{BH}), accretion luminosity (L_{disk}), and other related central engine properties of blazars detected by Fermi-LAT, Paliya et al. (2021) presented a catalog of 1030 sources for which the broadband SEDs are available. They collected the data from the Space Science Data Center (SSDC) SED builder tool and also involved the flux measurements given by the Second Swift X-ray Point Source catalog (2SXPS, Evans et al. 2020) and the 4FGL-DR2 catalog (Abdollahi et al. 2020). Then, the peak frequencies and corresponding fluxes for the synchrotron and IC components are estimated by fitting a second-degree polynomial to both peaks using the built-in function provided in the SSDC SED builder tool. Their whole catalog containing the SED-fitting results has been made public.⁵

However, their origin sample does not provide the classification. We thus cross-check this sample with 4FGL-DR3 (Fermi-LAT collaboration et al. 2022) and our previous work (Fan et al. 2016). Finally, we collect 572 γ -ray FSRQs for which the peak frequencies and peak luminosities of the synchrotron and EC components are given by Paliya et al. (2021) (and also the CD values). Besides, we likewise find 103 Blazar candidates of uncertain types (BCUs), i.e., blazar candidates of uncertain type (Ackermann et al. 2015), in the sample of Paliya et al. (2021). For the purpose of enlarging our sample, we classify these sources into UFs (BCUs classified as FSRQs) and UBs (BCUs classified as BL Lacs) by employing the empirical demarcation given by Chen (2018), namely, $\alpha_{\gamma}^{ph} = -0.127 \log L_{\gamma} + 8.18$, where α_{γ}^{ph} is the γ -ray photon index and L_{γ} denotes the γ -ray luminosity in units of erg s^{-1} . Based on this criterion, 47 UFs emerge. Therefore, we compile a catalog of 619 FSRQs overall. We list all the relevant data in Table 1. In this table, column (1) gives the 4FGL name; column (2) the redshift; column (3) the classification, where ‘‘FSRQ’’ denotes confirmed FSRQs and ‘‘UF’’ denotes BCU objects that are classified as FSRQs using the criterion from Chen (2018); column (4) the peak frequency of synchrotron emission in units of Hertz; column (5) the peak frequency of inverse Compton emission in units of Hertz; column (6) the peak luminosity of synchrotron component in units of erg s^{-1} ; column (7) the flux of the peak luminosity of the IC component in units of erg s^{-1} ;

column (8) the CD; column (9) the reference for columns (4)–(5), where P21 = Paliya et al. (2021); column (10) the γ -ray photon index adopted from 4FGL-DR3 (Fermi-LAT collaboration et al. 2022); column (11) the γ -ray luminosity in units of erg s^{-1} ; and column (12) the SF values derived in this work ($\log \sqrt{U_0} / \epsilon_0$).

3.2. The SF Distribution of FSRQs

Employing Equation (9), we obtain the SF values for our sample. We list the derived result in Table 1. The averaged value combining FSRQs and UFs is $\langle SF \rangle = 4.76 \pm 0.03 \text{ G}$. The histogram of distribution is presented in Figure 1. We label two ranges: The dashed blue area indicates the BLR and the dashed green indicates the DT region, respectively. $\mu = 4.72 \pm 0.03$ and $\sigma = 0.63 \pm 0.05$ have been obtained by performing the Gaussian fitting on a total of 619 sources. It is noticeable that our derived distribution is mainly located far beyond the BLR and within the DT. There are 570 sources (>92% of the total sample) located outside the BLR, i.e., $SF > 3.26 - 3.74 \text{ G}$. Consequently, our finding on the location of the γ -ray emission region supports the far-site scenario that seed photons are father out at parsec scales. Second, we also ascertain that the peak of the distribution is much closer to the DT region than the BLR, which is consistent with the conclusion of Zheng et al. (2017).

4. Discussion

For the past several decades, there have been various discussions on the topic of the emission region of γ -ray blazars. In the leptonic model, the GeV emission of blazars is produced by IC scattering of photons off of the same relativistic electrons in the jet that contribute to the synchrotron emission. For FSRQs, the seed photons for IC scattering are the synchrotron photons originating external to the jet, e.g., UV photons produced from the BLR, or IR photons produced from the DT. From there, two competing scenarios come forth—the near-site and far-site scenarios, the former based on the idea that the γ -ray emission region in relativistic jets of blazars is inside the BLR, at $\sim 0.1 - 1 \text{ pc}$ from the central engine, while the latter considers a region much farther away from the central engine at $\gg 1 \text{ pc}$.

To our knowledge, the distribution of seed photos can reflect the location of the γ -ray emission region; it is believed that seed photons are dissipated within the BLR in the near-site or dispersed close to the DT in the far-site scenario. The BLR produces UV photons while the DT produces IR photons.

Constraining the location of the γ -ray-emitting region can pave a path for us to better understand the IC radiative mechanism and the underlying peculiarity of blazars. If the IC emission dominated by the EC process originated within the BLR, a correlation between γ -ray and UV flares can be expected because the UV photons embedded in the BLR would

⁵ <http://www.ucm.es/blazars/engines>

Table 1
Sample of Fermi FSRQs

4FGL Name	Class	z	$\log \nu_{\text{syn}}^p$ (Hz)	$\log \nu_{\text{IC}}^p$ (Hz)	$\log L_{\text{syn}}^p$ (erg s^{-1})	$\log L_{\text{IC}}^p$ (erg s^{-1})	CD	Reference	$\alpha_{\gamma}^{\text{ph}}$	$\log L_{\gamma}$ (erg s^{-1})	SF (G)
(1)	(2)	(3)	(4)	(5)	(6)	(7)	(8)	(9)	(10)	(11)	(12)
J0001.5+2113	FSRQ	1.106	13.81	20.64	43.68	45.17	30.9	P21	2.659	46.78	6.92
J0004.3+4614	FSRQ	1.810	12.35	21.35	43.76	44.55	6.17	P21	2.585	46.63	4.4
J0010.6+2043	FSRQ	0.600	12.42	22.6	42.85	43	1.41	P21	2.318	45.21	2.9
J0030.6-0212	UF	1.804	12.59	21.48	43.94	44.99	11.22	P21	2.403	47.41	4.64
J0036.9+1832	UF	1.595	12.7	21.96	43.53	44.42	7.76	P21	2.385	46.52	4.19
J0042.2+2319	FSRQ	1.426	12.27	22.35	43.67	44.39	5.25	P21	2.322	46.56	3.29
...

Note. Column (1) gives the 4FGL name; column (2) the redshift; column (3) the classification, where “FSRQ” denotes the confirmed FSRQs and “UF” denotes BCU objects that are classified as FSRQs using the criterion from Chen (2018); column (4) the peak frequency of synchrotron emission in units of Hertz; column (5) the peak frequency of inverse Compton emission in units of Hertz; column (6) the peak luminosity of synchrotron component in units of erg s^{-1} ; column (7) the flux of peak luminosity of the IC component in units of erg s^{-1} ; column (8) the CD; column (9) the reference for columns (4)–(5), where P21 = Paliya et al. (2021); column (10) the γ -ray photon index adopted from 4FGL-DR3 (Fermi-LAT collaboration et al. 2022); column (11) the γ -ray luminosity in units of erg s^{-1} ; and column (12) the derived SF values in this work ($\log \sqrt{U_0}/\epsilon_0$).

(This table is available in its entirety in machine-readable form.)

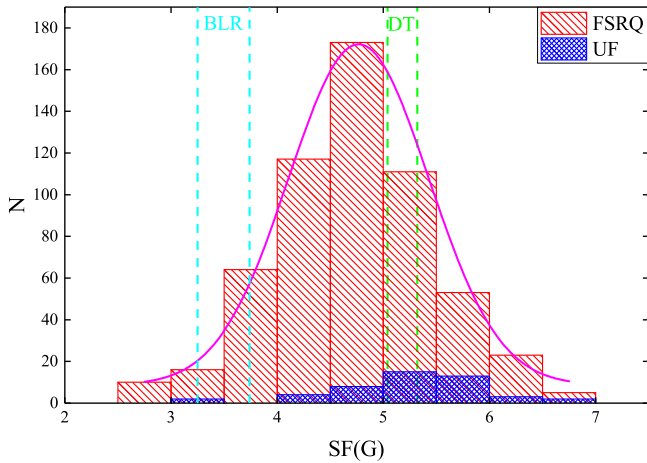


Figure 1. Histogram and Gaussian distribution of the derived SF in our sample. UFs denote the BCUs categorized as FSRQs (Chen 2018). The dashed blue and green areas signify the location of the BLR and DT, respectively.

be available for upscattering. Alternatively, for a far-site scenario, the IR photon fields are generated by the DT by reprocessing radiation from the accretion disk or by illumination from the jet synchrotron emission itself, and DT is a possible dominant source of seed photons for upscattering to higher energy (Arsioli & Chang 2018; Breiding et al. 2018). In this present work, we suggest that the seed photons that contribute to the γ -ray emission are produced in the DT region, thus supporting the far-site scenario. Many authors also identify this far-site scenario using different methods they propose (e.g., Sikora et al. 2008; Jorstad et al. 2010; Zheng et al. 2017; Kramarenko et al. 2022).

We consider that the decisive difference between the BLR and the DT lies in the energy of the seed photons (see, e.g., Dotson et al. 2012). If the γ -ray emission originates inside the BLR, the IC scattering of the BLR ultraviolet seed photons producing the γ -rays takes place at the Klein-Nishina (KN) regime. Whereas if the GeV emission originated farther out in the parsec-scale DT, the IC scattering of the infrared DT seed photons producing the γ -rays then comes about in the Thomson regime.

4.1. The Dominant Location of Seed Photons

In the jet frame, the comoving energy density for an isotropic photon field is $U' \approx (4/3)\Gamma^2 U$ and $U' \approx (3/4)\Gamma^{-2} U$ for the case of photons coming into the emitting region from behind (Dermer & Schlickeiser 1994). If the GeV emission originated within the BLR, the BLR photon field would be regarded as isotropic in the galaxy frame, then $U'_{\text{BLR}} \sim (4/3) \times 10^2 \Gamma^2 \text{ erg cm}^{-3}$. This consideration that the photon field is isotropic is also suitable for the DT seed photon energy density inside the BLR, i.e., $U'_{\text{DT}} \sim (4/3)\Gamma^2 \text{ erg cm}^{-3}$. Thus, for the near-site scenario, a factor of ~ 100 results from the comparison between the two above equations. In this sense, the seed photons of BLR (U'_{BLR}) are dominant.

On the other hand, for the far-site scenario, the BLR photons come into the emission region from behind, then $U'_{\text{BLR}} \sim (3/4) \times 10^{-8} \Gamma^{-2} \text{ erg cm}^{-3}$. The DT seed photon energy density remains unchanged. Consequently, if GeV emission is produced in the approach to the DT, the DT (U'_{DT}) dominates over U'_{BLR} .

Dotson et al. (2012) suggested that the electron cooling time plays an important role in the difference in the photon energy between BLR and DT, where γ -ray-emitting electron IC

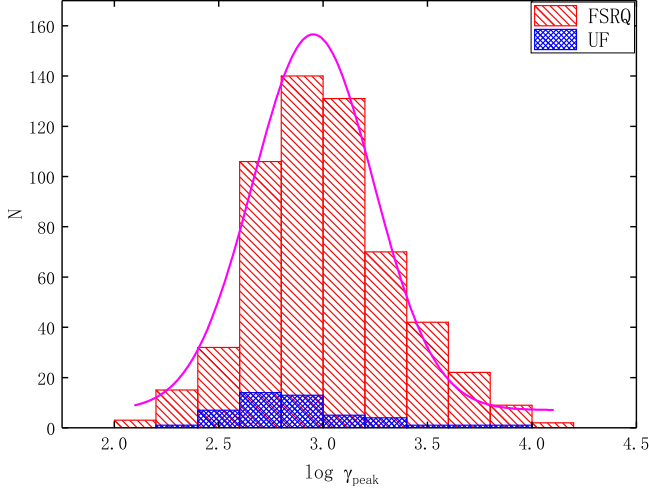


Figure 2. Distribution of the electron Lorentz factor. Gaussian fitting gives $\mu = 2.95 \pm 0.02$ and $\sigma = 0.28 \pm 0.02$. The entire range is in the TH regime.

cooling occurs (see also Cao & Wang 2013). Specifically, the energy dependence of the electron cooling time can be adopted to determine the regime where the electrons producing the GeV emission cooling, i.e., the γ -ray emission, takes place, whether that is in the Thomson (TH) regime or KN regime. Our derived result in this paper supports the IC scattering of the IR seed photons taking place in the Thomson regime, which leads to energy-dependent electron cooling times, demonstrated as faster cooling times for higher Fermi energy (Dotson et al. 2012; Finke 2013).

4.2. The Transition from the Thomson to Klein–Nishina Regime

In the TH regime, Abdo et al. (2010b) presented a tight correlation between the electrons' Lorentz factor and the EC peak frequency,

$$\gamma_{\text{peak}}^2 = \frac{3}{4} \frac{\nu_{\text{p}}^{\text{EC}}}{\nu_{\text{p}}^{\text{ext}} \Gamma} \frac{1+z}{\delta}, \quad (10)$$

where γ_{peak} denotes the Lorentz factor associated with the jet electrons emitting at the peak of synchrotron emission, Γ is the bulk Lorentz factor, and $\nu_{\text{p}}^{\text{ext}}$ is the peak frequency associated with the external photon field in the rest frame. We calculate the γ_{peak} for our 619 FSRQs, assuming that (i) the Doppler factor of $\delta \approx \Gamma$ for the relativistic jet is close to the line of sight in blazars with a viewing angle $\theta < 5^\circ$ (Jorstad et al. 2005; Dermer 2015); (ii) Chen (2018) shows that the median value of δ for a large sample of FSRQs is 10.7, thus we perform our calculation by taking $\delta = \Gamma = 10.7$; (iii) Spitzer observations indicates the typical peak frequency of IR dusty DT emission is $\nu_{\text{p}}^{\text{ext-IR}} \approx 3 \times 10^{13}$ Hz (Cleary et al. 2007; Ghisellini & Tavecchio 2009). Therefore, in the EC scenario, we obtain

$\langle \log \gamma_{\text{peak}} \rangle = 2.99 \pm 0.34$, ranging from 2.05 to 4.18. We plot the distribution in Figure 2.

The threshold from the TH to KN regime in the EC model is $\gamma_{\text{peak}} \Gamma h \nu_{\text{p}}^{\text{ext}} \gtrsim m_e c^2$, where h is the Planck constant and $m_e c^2$ is the electron energy. This criterion translates into $\log \gamma_{\text{peak}} \gtrsim 5.58$ (note that we adopt $\Gamma = 10.7$). Clearly, all sources are in the TH scattering regime, indicating that the EC scattering of the IR seed photons in DT producing the γ -rays occurs in the TH regime. This result supports our finding that the GeV emission for FSRQs originated around the DT location.

4.3. Correlations Associated with the Synchrotron and IC Component

In this work, we compute the seed photon factors for a large sample of FSRQs by employing their SED behavior. As a matter of course, we would like to probe some correlations such as the γ -ray luminosity against the synchrotron peak frequency or IC peak frequency.

The monochromatic luminosity is given by

$$L = 4\pi d_L^2 \nu f_\nu, \quad (11)$$

where f is the K -corrected flux density at the corresponding frequency ν , and d_L is the luminosity distance. The data on the γ -ray emission (e.g., the photon index $\alpha_\gamma^{\text{ph}}$ and γ -ray flux) are taken from Fermi-LAT collaboration et al. (2022). Using this equation, we can obtain the γ -ray luminosities. We list them in column (11) of Table 1.

The comparisons of the γ -ray luminosity against synchrotron peak frequency and photon index versus IC peak frequency are shown in Figure 3. Two strong correlations are found. The best fit for the synchrotron component is $\log L_\gamma = -(0.74 \pm 0.07) \log \nu_{\text{syn}}^{\text{p}} + (55.74 \pm 0.96)$ with a correlation coefficient $r = -0.37$ and a chance probability of $p < 10^{-4}$ (see the left panel). Similarly, Fan et al. (2016) found a tight anticorrelation between $\log \nu_{\text{syn}}^{\text{p}}$ and $\log L_\gamma$ for 999 γ -ray-loud blazars, described as $\log L_\gamma = -(0.29 \pm 0.02) \log \nu_{\text{syn}}^{\text{p}} + (49.58 \pm 0.35)$ with $r = -0.32$ and $p < 10^{-4}$. Fossati et al. (1998) also show the highly significant relation that the synchrotron peak is increasing with decreasing luminosity. The anticorrelation between these two quantities is believed to be due to the strong beam in the radio emission. Nieppola et al. (2008) found that the radio Doppler factor would be larger at low synchrotron peaked blazars and smaller at high synchrotron peaked blazars. This leads to higher beaming in low peaked sources and lower beaming in highly peaked sources. Thus, an anticorrelation between the peak frequency and radio luminosity can be expected. Meanwhile, the γ -ray luminosity and radio luminosity for Fermi blazars are strongly correlated (see, e.g., Fan et al. 2016; Zhang & Fan 2018, and references therein). Therefore, an anticorrelation between $\log \nu_{\text{syn}}^{\text{p}}$ and $\log L_\gamma$ can be well explained.

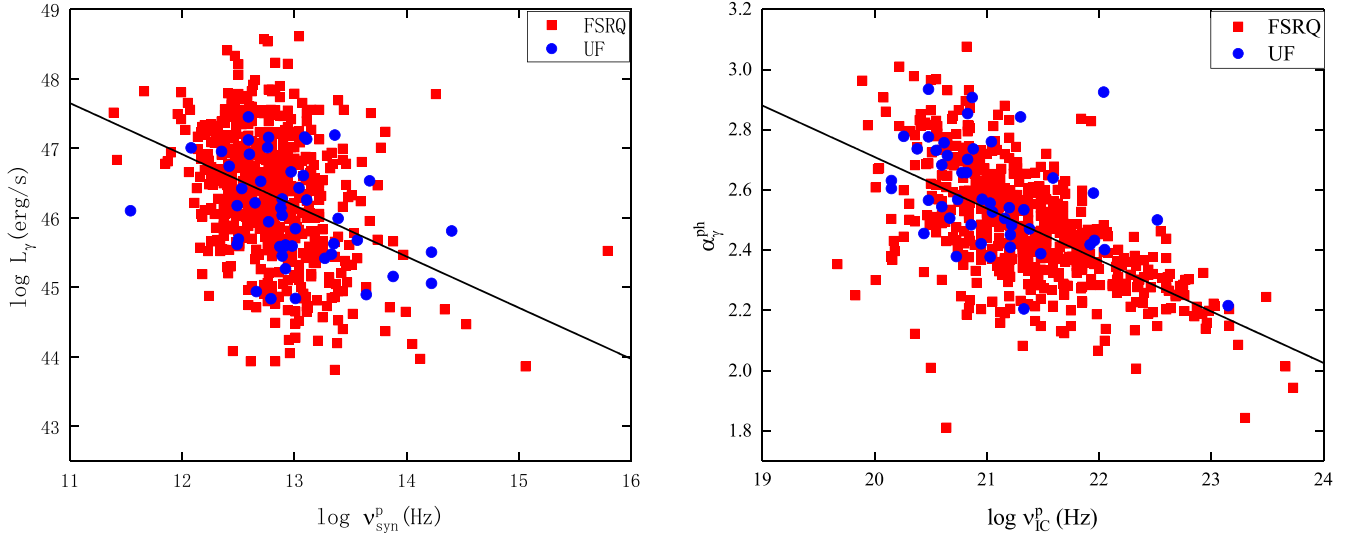


Figure 3. Plots of the γ -ray luminosity vs. the peak frequency of the synchrotron emission (left panel) and the photon index against the peak frequency of the IC (right panel). The best fit gives $\log L_\gamma = -(0.74 \pm 0.07)\log \nu_{\text{syn}}^p + (55.74 \pm 0.96)$ with $r = -0.37$ and $p < 10^{-4}$ for the synchrotron component, and $\log \nu_{\text{EC}}^p = -(2.06 \pm 0.11)\alpha_\gamma^{\text{ph}} + (26.44 \pm 0.28)$ with $r = -0.59$ and $p \sim 0$ for the IC component, respectively.

On the other hand, the right panel demonstrates a significantly negative correlation in the $\alpha_\gamma^{\text{ph}} - \log \nu_{\text{IC}}^p$ plane, namely $\log \nu_{\text{EC}}^p = -(2.06 \pm 0.11)\alpha_\gamma^{\text{ph}} + (26.44 \pm 0.28)$ with $r = -0.59$ and $p \sim 0$. Because sometimes there are not sufficient quasi-simultaneous data to construct the IC bump for a large sample, we can make use of this relation to estimate the EC peak frequency when a photon index is given for FSRQs. Abdo et al. (2010b) also derived the correlation between the IC peak and photon index for 48 sources, which, owing to their quasi-simultaneous nature on the GeV band, are available for conducting SED fitting and obtaining the IC peak frequency. The best fit is $\log \nu_{\text{IC}}^p = -4\alpha_\gamma^{\text{ph}} + 31.6$. Notably, the slope of the $\alpha_\gamma^{\text{ph}} - \log \nu_{\text{IC}}^p$ plane we obtain in this work is ~ -2 and -4 was also found in Abdo et al. (2010b). We consider this to be due to the collected sample in Abdo et al. (2010b) being small, and besides, most principally, combining FSRQs and BL Lacs. Our present work only takes FSRQs into account, thus the slope will flatten because the FSRQs normally have a larger γ -ray photon index.

Similarly, Arsioli & Chang (2018) ascertained a tight relation displaying $\alpha_\gamma^{\text{ph}} = -0.229 \log \nu_{\text{IC}}^p + 7.34$ for a limited sample of radio-Planck sources with good measures for the IC parameter. This tight connection between $\alpha_\gamma^{\text{ph}}$ and $\log \nu_{\text{IC}}^p$ indicates that blazars are associated with the steepest γ -ray sources in the 0.1–100 GeV band with the IC peaks around the MeV band. Ghisellini et al. (2009) inferred that reducing the γ -ray flux threshold may detect blazars with a steeper spectral index and lower luminosity (see also Abdo et al. 2009b).

Finally, we remark that the correlations between the γ -ray behavior versus the synchrotron/IC components shown in

Figure 3 are natural because both components depend linearly on the relativistic electrons within the jet that are producing synchrotron emission and upscattering the low-energy photons into γ -rays (see the detail discussion in Giommi et al. 2012, 2013).

It should be noted that the relationships associated with the γ -ray behavior and both the synchrotron and IC contributions are intrinsic and do not depend on the redshift. Fossati et al. (1998) discovered that the correlations persist even if the redshift effect is subtracted, which elicited the question of whether the spectral sequence or “blazar sequence” (a unified scheme whereby blazar continua can be described by a family of analytic curves with the source luminosity as the fundamental parameter) actually exists. Finke (2013) probes into the Compton dominance (called γ -ray dominance in the past), the ratio of the peak of the Compton to the synchrotron peak luminosities, which is essentially a redshift-independent quantity and thus crucial to answering this question. Subsequently, they found that a correlation exists between the CD and the peak frequency of the synchrotron component for all blazars in their sample, including ones with an unknown redshift. In this work, to confirm this verdict, we also analyze the correlation of CD against ν_{syn}^p for our FSRQ sample. An anticorrelation is obtained, described as $\log \text{CD} = -(0.20 \pm 0.03)\log \nu_{\text{syn}}^p + (3.08 \pm 0.50)$ with $r = -0.20$ and $p = 6.32 \times 10^{-7}$. This plot is shown in Figure 4.

Yang et al. (2022) revisit the correlation for a large sample of 255 blazars from 4FGL with available Doppler factors, drawing the conclusion that the observed radio, X-ray, γ -ray, and synchrotron peak luminosity are all anticorrelated with the peak

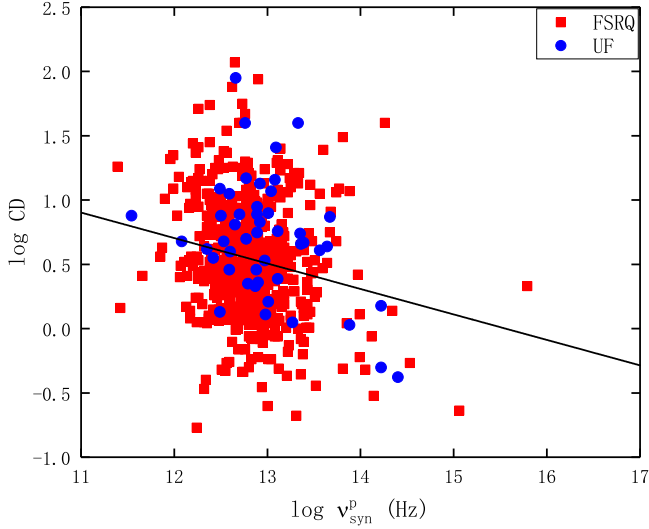


Figure 4. Plot of Compton dominance vs. synchrotron peak frequency. The best fit gives $\log CD = -(0.20 \pm 0.03)\log \nu_{\text{syn}}^p + (3.08 \pm 0.50)$ with $r = -0.20$ and $p = 6.32 \times 10^{-7}$.

frequency, but the debeamed luminosity is positively correlated with the debeamed peak frequency. This implies that those anticorrelations are perhaps due to a selection effect or a beaming effect (see also Chen et al. 2021).

4.4. VHE FSRQs

Interestingly, Acharyya et al. (2021) investigate six bright FSRQs showing very high-energy (VHE) photon emission. The VHE photons are characterized by having an energy $E_\gamma \geq 20$ GeV in the rest frame of a source, and these FSRQs are also known as TeV sources.⁶ They found the γ -ray emission region for these six bright FSRQs are beyond the BLR and farther out in the DT, supporting the far-site scenario. We cross-checked these six FSRQs and find they are all in our sample with average daily fluxes of $10^{-6} \text{ cm}^{-2} \text{ s}^{-1}$ within 1σ uncertainties above 100 MeV. They are CTA 102, B2 1520+31, PKS 1510–089, PKS 1502+106, PKS 1424–41, and PKS 0454–234, and their SF values are 4.93, 4.80, 5.15, 4.89, 5.08, and 5.04, respectively. In other words, they are all between the peak of the SF distribution and the range of DT, indicating the γ -ray location of these sources is far beyond the BLR and very close to (or, say, around) the DT region.

Previous observations of VHE photons also show that the γ -ray emission originated outside the BLR (e.g., Liu & Bai 2006). However, Böttcher & Els (2016) pointed out that the opacity constraints derived can be evaded by resorting to multizone models where the production regions of GeV and VHE emission are not cospatial because the VHE photons observed are emitted at large distances from the SMBH.

⁶ <http://tevcat2.uchicago.edu/>

Therefore, this characteristic feature is likely to challenge the simple one-zone leptonic emission model, the standard and most widely used version of the leptonic model, which assumes there is only one leptonic plasma-filled zone responsible for the synchrotron and IC emission of a blazar.

Based on our findings, we suggest that FSRQs whose seed photons are produced around the DT are probably TeV sources, showing very high energy ($E_\gamma \geq 20$ GeV). Another interpretation is that if the emission region is located far beyond the BLR, the VHE photons can avoid severe γ – γ absorption and the KN effect would be weak in the VHE spectrum until the energy is far larger than 10^{25} Hz (e.g., Cao & Wang 2013).

4.5. Can SF Likewise Imply the Region of Neutrino Emission?

On 2017 September 22, the IceCube Neutrino Observatory detected a high-energy ($E_\nu \gtrsim 290$ TeV) muon-track neutrino event (IceCube-170922A) from the flaring blazar TXS 0506+056 (IceCube Collaboration et al. 2018a), located at a redshift of $z = 0.3365$ (Paiano et al. 2018). A follow-up analysis of IceCube archival data reported a $\sim 3.5\sigma$ excess of 13 ± 5 neutrino events in the range of 32 TeV–3.6 PeV to be coincident with the flaring state of the blazar TXS 0506+056 during a ~ 6 month period in 2014–2015, yielding the first ever $\sim 3\sigma$ high-energy neutrino source association (IceCube Collaboration et al. 2018b). Neutrinos are produced in photopion ($p\gamma$, $p + \gamma \rightarrow \pi^+ + n$) or hadronic (pp , $p + p \rightarrow X + N_\pi \pi^\pm$, here N_π stands for the pion multiplicity) interactions of protons and nuclei.

Beforehand, many authors have proposed that blazars may accelerate protons to very high energies and may thus be cosmic neutrino-emitter sources. Notably, flares are ideal periods for neutrino production in blazars (e.g., Zhang et al. 2020). During the flares, the density of the target photon field for photomeson interactions with the hadrons within the jet would be enhanced along with the injection rate of accelerated protons. This leads to the neutrino luminosity being significantly reinforced relative to the γ -ray luminosity, namely $L_\nu \propto L_\gamma^\alpha$, where $\alpha \sim 1.5$ – 2 (Murase et al. 2014; Murase & Waxman 2016; Petropoulou et al. 2016).

Neutrino production is expected to be much more efficient in FSRQs than in BL Lacs due to the higher powers and existence of external photon fields (Atoyan & Dermer 2003). The nuclear region of FSRQs is naturally abundant in photons, providing an ideal environment for high-energy neutrinos to originate from photohadronic interactions. Coincidentally, Padovani et al. (2019) pointed out that TXS 0506+056 is a masquerading BL Lac object with a hidden BLR of luminosity $\approx 5 \times 10^{43} \text{ erg s}^{-1}$ and a standard accretion disk, i.e., intrinsically an FSRQ.

At present, a popular idea for the location of neutrino emission is that the neutrinos and γ -rays are produced in

the same region. Cospacial production is in general expected if the neutrino emission is correlated with the γ -ray flare, and many studies have reached this conclusion on the 2017 flare of TXS 0506+056 (i.e., a single-zone model; see, e.g., Ansoldi et al. 2018; Keivani et al. 2018; Cerruti et al. 2019; Gao et al. 2019; Plavin et al. 2020). In contrast, Xue et al. (2019) proposed a two-zone photohadronic model for the flare of TXS 0506+056 and demonstrated there are two distinct emitting regions, namely a compact region within the BLR responsible for the neutrino emission and γ -ray emission, and another region that is beyond the BLR accounting for the synchrotron emission. In this case, large amounts of neutrinos could be produced by the standard $p\gamma$ model in which all of the emission is cospacially produced. Righi et al. (2020) analyzed the SED of neutrinos and the diffuse flux for FSRQs in two different regions as well.

Thus, if we consider that neutrino emission occurs in the same region as photon emission, there are accordingly two scenarios describing the location of neutrinos, the near-site and far-site scenario, as aforementioned. As a consequence, we suggest that the SF can also be an indicator of the location of the neutrino-emitting region.

We employ the single-zone model as the same framework for deriving SF. In this model, neutrinos and γ -rays are coproduced inside the blazar blob through $p\gamma$ interactions. High-energy protons in the emitting region interact with photons to produce charged and neutral pions, which lead to comparable fluxes of neutrino emission and γ -ray emission. If the target photons are comoving with a jet with bulk Lorentz factor Γ , the predicted neutrino energy ϵ_ν for all flavors can be estimated via (Oikonomou 2022)

$$\epsilon_\nu \approx 100 \text{ PeV} (40 \text{ eV} / \epsilon_\gamma) (\Gamma / 10)^2 (1 + z)^2, \quad (12)$$

where ϵ_γ is the photon energy. Therefore, given the value of the external photon field energy density U_0 for a source, we can obtain the characteristic energy ϵ_0 for external seed photons from our derived SF and compute the photon energy via $\epsilon_\gamma = \gamma_{\text{peak}}^2 \epsilon_0$.

Our present work shows that the seed photons are probably originated from the DT region. The SF values span from 5.04 to 5.32 G, and 93 sources in our sample are located in this range. If we consider the neutrino emission is also produced from DT, i.e., a far-site scenario, we obtain the neutrino energy to be $\epsilon_\nu \simeq 5.62$ to 850.33 PeV with a median value of 193.20, using $\epsilon_{0,\text{DT}} = 5.7 \times 10^{-7}$ and Equation (12). The distribution of ϵ_ν for the far-site scenario is displayed in Figure 5.

In comparison with the PeV neutrino production, ~ 0.1 – 1 EeV neutrinos are produced by way of interactions between protons and IR photons from the dust torus. The lower limit of neutrino energy in these circumstances can be roughly

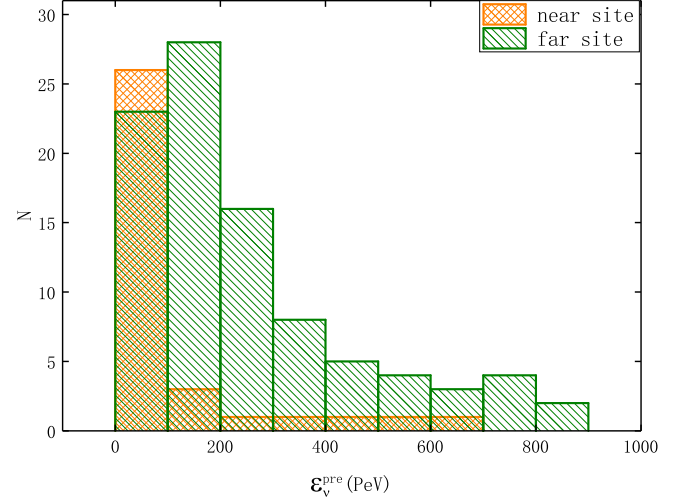


Figure 5. Distributions of the predicted neutrino energy in all flavors for the near-site and far-site scenarios, respectively.

estimated following Murase et al. (2014)

$$\epsilon_\nu = 0.066 \text{ EeV} (T_{\text{IR}} / 500 \text{ K})^{-1}, \quad (13)$$

where T_{IR} refers to the aforementioned temperature of the dust torus. In like manner, we adopt $T_{\text{IR}} = 1200$. Hence, we ascertain $\epsilon_\nu \gtrsim 0.0275$ EeV.

By contrast, if we consider the near-site scenario, SF = 3.26–3.74 G and there are 34 FSRQs in this region. The characteristic photon energy for the BLR is $\epsilon_{0,\text{BLR}} = 3 \times 10^{-5}$, which results in $\epsilon_\nu \simeq 2.24$ – 604.34 PeV with a median value of 60.47 (see the distribution in Figure 5).

The neutrino energy we achieve is typically higher than 1 PeV and the Glashow resonance energy at 6.3 PeV (for electron antineutrinos). We conclude that the external radiation field plays an important role in PeV–EeV neutrino production. The predicted ϵ_ν distributions for the near-site and far-site scenarios we propose in this work that correspond to the γ -ray emission region are comparable. Thus, these two frameworks could be both potential for the production of neutrinos. This remains to be tested during long-lived blazars flares.

All in all, blazars are the most well-known class of extragalactic high-energy particle accelerators, especially of FSRQs, because they possess an efficient accretion disk and a dense ultraviolet photon field surrounding the black hole, which are optimal for the production of \gg PeV-energy neutrinos. We propose the seed photon factors can also be an indicator for the neutrino emission location because the idea that neutrinos and γ -rays are coproduced in the same region is generally accepted.

5. Conclusion

In this paper, we constrain the dissipative location of the γ -ray emission for a large sample of 619 FSRQs, including 572 confirmed FSRQs and 47 BCU-FSRQ candidates by means of the seed photon factor approach proposed by Georganopoulos et al. (2012). This method is tightly associated with the SED behavior, and the SF can be simply derived as long as the peak frequency and peak luminosity of the synchrotron along with IC components are available. We take these SED data directly from Paliya et al. (2021). We stress that this seed photon approach is only valid for the EC scattering model, thus it is applicable to discuss the GeV emission of FSRQ-type blazars. We find that the location of γ -rays is far beyond the BLR and close to the DT, which supports the far-site scenario. Meanwhile, we discuss the correlations associated with synchrotron emission and EC scattering. We also shed new light on the production region of neutrino emission. The main conclusions of this work are as follows:

1. The region of γ -ray emission of FSRQs is farther out at parsec scales from the SMBH where the molecular torus IR emission dominates, which can be illustrated by two aspects: (i) The SF distribution is mainly located far beyond the BLR and verges on the DT region. (ii) All sources are in the Thomson scattering regime, indicating that the EC scattering of IR seed photons in DT producing the γ -rays occurs in the TH regime, which is evidence that the GeV emission for FSRQs originated around the DT region. Besides, the DT dominance also supports energy-dependent electron cooling times, appearing as faster cooling times for higher Fermi energy.
2. FSRQs with their seed photons produced in the range of DT are probably TeV sources, emitting very high energy with $E_\gamma \geq 20$ GeV (VHE). The reason is that if the emission region is located far beyond the BLR, the VHE photons can avoid the severe γ - γ absorption and the KN effect would be weak in the VHE spectrum until the energy is much larger than 10^{25} Hz.
3. An expected anticorrelation between the synchrotron peak frequency and γ -ray luminosity has been verified for our sample because the γ -ray luminosity and radio luminosity for Fermi-detected blazars are strongly correlated, leading to higher beaming in low peaked sources and lower beaming in highly peaked sources.
4. We suggest that our derived SF can also be an indicator to estimate the location of neutrino emission. We also propose that two similar scenarios could be discussed—the near-site and far-site models—in consideration of the neutrinos and γ -rays being cospatially produced within the same region. We compute the predicted neutrino energy for the overall sample and find ϵ_ν for two frameworks are comparable with $\gg 1$ PeV, satisfying our general expectation that blazars are optimal production

factories for PeV–EeV energy neutrinos in the extragalactic γ -ray sky.

We are grateful to the anonymous referee for valuable comments and constructive suggestions, which helped us to improve the manuscript. This work is partially supported by the National Natural Science Foundation of China (NSFC U2031201, NSFC 11733001, U2031112), Guangdong Major Project of Basic and Applied Basic Research (grant No. 2019B030302001). D.Y.H. acknowledges support from Guangzhou University and the “Challenge Cup” National Undergraduate Curricular Academic Science and Technology Works Competition (grant 2022TZBNAI2001). Z.Y.P. acknowledges support from the National Science Foundation for Young Scientists of China (grant 12103012), and China Postdoctoral Science Foundation (grant 2022M710868). We also acknowledge the science research grants from the China Manned Space Project with No. CMS-CSST-2021-A06 and the support for Astrophysics Key Subjects of Guangdong Province and Guangzhou City.

ORCID iDs

Zhiyuan Pei  <https://orcid.org/0000-0002-4970-3108>,

Junhui Fan  <https://orcid.org/0000-0002-5929-0968>,

References

- Abdo, A. A., Ackermann, M., Ajello, M., et al. 2009a, *ApJS*, 183, 46
 Abdo, A. A., Ackermann, M., Ajello, M., et al. 2009b, *ApJ*, 700, 597
 Abdo, A. A., Ackermann, M., Ajello, M., et al. 2010a, *ApJ*, 720, 912
 Abdo, A. A., Ackermann, M., Agudo, I., et al. 2010b, *ApJ*, 716, 30
 Abdo, A. A., Ackermann, M., Ajello, M., et al. 2010c, *ApJS*, 188, 405
 Abdo, A. A., Ackermann, M., Ajello, M., et al. 2010d, *ApJ*, 715, 429
 Abdo, A. A., Ackermann, M., Ajello, M., et al. 2010e, *ApJL*, 714, L73
 Abdollahi, S., Acero, F., Ackermann, M., et al. 2020, *ApJS*, 247, 33
 Acero, F., Ackermann, M., Ajello, M., et al. 2015, *ApJS*, 218, 23
 Acharyya, A., Chadwick, P. M., & Brown, A. M. 2021, *MNRAS*, 500, 5297
 Ackermann, M., Ajello, M., Atwood, W. B., et al. 2015, *ApJ*, 810, 14
 Ackermann, M., Ajello, M., Baldini, L., et al. 2010, *ApJ*, 721, 1383
 Agudo, I., Marscher, A. P., Jorstad, S. G., et al. 2011, *ApJL*, 735, L10
 Ajello, M., Angioni, R., Axelsson, M., et al. 2020, *ApJ*, 892, 105
 Ansoldi, S., Antonelli, L. A., Arcaro, C., et al. 2018, *ApJL*, 863, L10
 Arbeiter, C., Pohl, M., & Schlickeiser, R. 2002, *A&A*, 386, 415
 Arsioli, B., & Chang, Y. L. 2018, *A&A*, 616, A63
 Atoyan, A. M., & Dermer, C. D. 2003, *ApJ*, 586, 79
 Atwood, W. B., Abdo, A. A., Ackermann, M., et al. 2009, *ApJ*, 697, 1071
 Bentz, M. C., Peterson, B. M., Netzer, H., Pogge, R. W., & Vestergaard, M. 2009, *ApJ*, 697, 160
 Błażejowski, M., Sikora, M., Moderski, R., & Madejski, G. M. 2000, *ApJ*, 545, 107
 Blumenthal, G. R., & Gould, R. J. 1970, *RvMP*, 42, 237
 Böttcher, M. 1999, *ApJL*, 515, L21
 Böttcher, M., & Els, P. 2016, *ApJ*, 821, 102
 Breiding, P., Georganopoulos, M., & Meyer, E. T. 2018, *ApJ*, 853, 19
 Burd, P. R., Kohlhepp, L., Wagner, S. M., et al. 2021, *A&A*, 645, A62
 Cao, G., & Wang, J.-C. 2013, *MNRAS*, 436, 2170
 Cerruti, M., Zech, A., Boisson, C., et al. 2019, *MNRAS*, 483, L12
 Chen, L. 2018, *ApJS*, 235, 39
 Chen, Y., Gu, Q., Fan, J., et al. 2021, *ApJ*, 913, 93

- Cleary, K., Lawrence, C. R., Marshall, J. A., Hao, L., & Meier, D. 2007, *ApJ*, **660**, 117
- Coppi, P. S., & Blandford, R. D. 1990, *MNRAS*, **245**, 453
- Dermer, C. D. 2015, *Mem. Soc. Astron. Italiana*, **86**, 13
- Dermer, C. D., & Schlickeiser, R. 1994, *ApJS*, **90**, 945
- Dondi, L., & Ghisellini, G. 1995, *MNRAS*, **273**, 583
- Dotson, A., Georganopoulos, M., Kazanas, D., & Perlman, E. S. 2012, *ApJL*, **758**, L15
- Evans, P. A., Page, K. L., Osborne, J. P., et al. 2020, *ApJS*, **247**, 54
- Fan, J., Yang, J. H., Zhang, J.-Y., et al. 2013, *PASJ*, **65**, 25
- Fan, J.-H., Huang, Y., He, T.-M., et al. 2009, *PASJ*, **61**, 639
- Fan, J. H., Kurtanidze, S. O., Liu, Y., et al. 2021, *ApJS*, **253**, 10
- Fan, J.-H., Romero, G. E., Wang, Y.-X., & Zhang, J.-S. 2005, *ChJAA*, **5**, 457
- Fan, J. H., Yang, J. H., Liu, Y., et al. 2016, *ApJS*, **226**, 20
- Fermi-LAT collaboration, Abdollahi, S., et al. 2022, *ApJS*, **260**, 53
- Finke, J. D. 2013, *ApJ*, **763**, 134
- Foschini, L. 2011, *RAA*, **11**, 1266
- Fossati, G., Maraschi, L., Celotti, A., Comastri, A., & Ghisellini, G. 1998, *MNRAS*, **299**, 433
- Gao, S., Fedynitch, A., Winter, W., & Pohl, M. 2019, *NatAs*, **3**, 88
- Georganopoulos, M., Meyer, E. T., & Fossati, G. 2012, arXiv:1202.6193
- Ghisellini, G. 1993, *ApJ*, **407**, 65
- Ghisellini, G., Celotti, A., Fossati, G., Maraschi, L., & Comastri, A. 1998, *MNRAS*, **301**, 451
- Ghisellini, G., Maraschi, L., & Tavecchio, F. 2009, *MNRAS*, **396**, L105
- Ghisellini, G., & Tavecchio, F. 2008, *MNRAS*, **386**, L28
- Ghisellini, G., & Tavecchio, F. 2009, *MNRAS*, **397**, 985
- Ghisellini, G., Tavecchio, F., Foschini, L., & Ghirlandola, G. 2011, *MNRAS*, **414**, 2674
- Ghisellini, G., Tavecchio, F., Foschini, L., et al. 2010, *MNRAS*, **402**, 497
- Giommi, P., Padovani, P., & Polenta, G. 2013, *MNRAS*, **431**, 1914
- Giommi, P., Padovani, P., Polenta, G., et al. 2012, *MNRAS*, **420**, 2899
- Harvey, A. L. W., Georganopoulos, M., & Meyer, E. T. 2020, *NatCo*, **11**, 5475
- IceCube Collaboration, Aartsen, M. G., Ackermann, M., et al. 2018a, *Sci*, **361**, 147
- IceCube Collaboration, Aartsen, M. G., Ackermann, M., et al. 2018b, *Sci*, **361**, eaat1378
- Jorstad, S. G., Marscher, A. P., Larionov, V. M., et al. 2010, *ApJ*, **715**, 362
- Jorstad, S. G., Marscher, A. P., Lister, M. L., et al. 2005, *AJ*, **130**, 1418
- Jorstad, S. G., Marscher, A. P., Mattox, J. R., et al. 2001, *ApJ*, **556**, 738
- Kaspi, S., Brandt, W. N., Maoz, D., et al. 2007, *ApJ*, **659**, 997
- Keivani, A., Murase, K., Petropoulou, M., et al. 2018, *ApJ*, **864**, 84
- Kishimoto, M., Hönig, S. F., Antonucci, R., et al. 2011, *A&A*, **536**, A78
- Kramarenko, I. G., Pushkarev, A. B., Kovalev, Y. Y., et al. 2022, *MNRAS*, **510**, 469
- Larionov, V. M., Jorstad, S. G., Marscher, A. P., et al. 2008, *A&A*, **492**, 389
- Lindfors, E. J., Valtaoja, E., & Türler, M. 2005, *A&A*, **440**, 845
- Liu, H. T., & Bai, J. M. 2006, *ApJ*, **653**, 1089
- Madau, P., Ghisellini, G., & Persic, M. 1987, *MNRAS*, **224**, 257
- Malmrose, M. P., Marscher, A. P., Jorstad, S. G., Nikutta, R., & Eitzur, M. 2011, *ApJ*, **732**, 116
- Marscher, A., Jorstad, S. G., Larionov, V. M., Aller, M. F., & Lähteenmäki, A. 2011, *A&A*, **32**, 233
- Marscher, A. P., Jorstad, S. G., Larionov, V. M., et al. 2010, *ApJL*, **710**, L126
- Meyer, M., Scargle, J. D., & Blandford, R. D. 2019, *ApJ*, **877**, 39
- Murase, K., Inoue, Y., & Dermer, C. D. 2014, *PhRvD*, **90**, 023007
- Murase, K., & Waxman, E. 2016, *PhRvD*, **94**, 103006
- Nalewajko, K., Begelman, M. C., & Sikora, M. 2014, *ApJ*, **789**, 161
- Nieppola, E., Valtaoja, E., Tornikoski, M., Hovatta, T., & Kotiranta, M. 2008, *A&A*, **488**, 867
- Oikonomou, F. 2022, arXiv:2201.05623
- Padovani, P., Oikonomou, F., Petropoulou, M., Giommi, P., & Resconi, E. 2019, *MNRAS*, **484**, L104
- Paiano, S., Falomo, R., Treves, A., & Scarpa, R. 2018, *ApJL*, **854**, L32
- Paliya, V. S., Domínguez, A., Ajello, M., Olmo-García, A., & Hartmann, D. 2021, *ApJS*, **253**, 46
- Pei, Z., Fan, J., Bastieri, D., Yang, J., & Xiao, H. 2020a, *SCPMA*, **63**, 259511
- Pei, Z., Fan, J., Yang, J., Huang, D., & Li, Z. 2022, *ApJ*, **925**, 97
- Pei, Z.-Y., Fan, J.-H., Bastieri, D., Sawangwit, U., & Yang, J.-H. 2019, *RAA*, **19**, 070
- Pei, Z.-Y., Fan, J.-H., Bastieri, D., et al. 2020b, *RAA*, **20**, 025
- Pei, Z. Y., Fan, J. H., Liu, Y., et al. 2016, *Astrophysics and Space Science*, **361**, 237
- Petropoulou, M., Giannios, D., & Sironi, L. 2016, *MNRAS*, **462**, 3325
- Planck Collaboration, Ade, P. A. R., Aghanim, N., et al. 2014, *A&A*, **571**, A1
- Plavin, A., Kovalev, Y. Y., Kovalev, Y. A., & Troitsky, S. 2020, *ApJ*, **894**, 101
- Poutanen, J., & Stern, B. 2010, *ApJL*, **717**, L118
- Pozo Nuñez, F., Haas, M., Chini, R., et al. 2014, *A&A*, **561**, L8
- Righi, C., Palladino, A., Tavecchio, F., & Vissani, F. 2020, *A&A*, **642**, A92
- Romero, G. E., Cellone, S. A., Combi, J. A., & Andruchow, I. 2002, *A&A*, **390**, 431
- Rybicki, G. B., Lightman, A. P., & Tayler, R. J. 1981, *Natur*, **289**, 729
- Savolainen, T., Homan, D. C., Hovatta, T., et al. 2010, *A&A*, **512**, A24
- Scarpa, R., & Falomo, R. 1997, *A&A*, **325**, 109
- Sikora, M., Begelman, M. C., & Rees, M. J. 1994, *ApJ*, **421**, 153
- Sikora, M., Moderski, R., & Madejski, G. M. 2008, *ApJ*, **675**, 71
- Suganuma, M., Yoshii, Y., Kobayashi, Y., et al. 2006, *ApJ*, **639**, 46
- Tavecchio, F., & Ghisellini, G. 2008, *MNRAS*, **386**, 945
- Tavecchio, F., Ghisellini, G., Bonnoli, G., & Ghirlandola, G. 2010, *MNRAS*, **405**, L94
- Tavecchio, F., Maraschi, L., & Ghisellini, G. 1998, *ApJ*, **509**, 608
- Urry, C. M., & Padovani, P. 1995, *PASP*, **107**, 803
- Wagner, S. J., Camenzind, M., Dreissigacker, O., et al. 1995, *A&A*, **298**, 688
- Wills, B. J., Wills, D., Breger, M., Antonucci, R. R. J., & Barvainis, R. 1992, *ApJ*, **398**, 454
- Xiao, H., Fan, J., Yang, J., et al. 2019, *SCPMA*, **62**, 129811
- Xue, R., Liu, R.-Y., Petropoulou, M., et al. 2019, *ApJ*, **886**, 23
- Yan, D., Wu, Q., Fan, X., Wang, J., & Zhang, L. 2018, *ApJ*, **859**, 168
- Yang, W. X., Wang, H. G., Liu, Y., et al. 2022, *ApJ*, **925**, 120
- Zhang, L., Chen, S., Xiao, H., Cai, J., & Fan, J. 2020, *ApJ*, **897**, 10
- Zhang, L. X., & Fan, J. H. 2018, *Astrophysics and Space Science*, **363**, 142
- Zheng, Y. G., Yang, C. Y., Zhang, L., & Wang, J. C. 2017, *ApJS*, **228**, 1